ELSEVIER

Journal of Fluids and Structures 23 (2007) 665–680

JOURNAL OF FLUIDS AND STRUCTURES

www.elsevier.com/locate/jfs

Limit cycle oscillations of rectangular cantilever wings containing cubic nonlinearity in an incompressible flow

B. Ghadiri*, M. Razi

Department of Mechanical Engineering, School of Engineering, Tarbiat Modares University, P.O. Box 14115-143, Tehran, Iran

Received 14 March 2006; accepted 31 October 2006
Available online 26 December 2006

Abstract

Limit cycle oscillations (LCO) as well as nonlinear aeroelastic analysis of rectangular cantilever wings with a cubic nonlinearity are investigated. Aeroelastic equations of a rectangular cantilever wing with two degrees of freedom in an incompressible potential flow are presented in the time domain. The harmonic balance method is modified to calculate the LCO frequency and amplitude for rectangular wings. In order to verify the derived formulation, flutter boundaries are obtained via a linear analysis of the derived system of equations for five different cases and compared with experimental data. Satisfactory results are gained through this comparison. The problem of finding the LCO frequency and amplitude is solved via applying the two methods discussed for two different cases with hardening cubic nonlinearities. The results from first-, third- and fifth-order harmonic balance methods are compared with the results of an exact numerical solution. A close agreement is obtained between these harmonic balance methods and the exact numerical solution of the governing aeroelastic equations. Finally, the nonlinear aeroelastic analysis of a rectangular cantilever wing with a softening nonlinearity is studied.

Keywords: Cubic nonlinearity; Harmonic balance method; Limit cycle oscillations; Numerical solution; Rectangular cantilever wing

1. Introduction

Aeroelasticity is defined as the interaction of aerodynamics, elasticity and dynamics. Classical theories of aeroelasticity assume that the aerodynamic and structural forces are linear. For many decades, the classical approach has been successful in providing approximate estimates of aircraft response to gusts, turbulence and external excitation. The flutter boundaries are often quite accurately predicted when compared to flight test results. On the other hand, these classical methods are unable to capture phenomena arising from structural and aerodynamic nonlinearities.

Aerodynamic nonlinearities are often encountered at transonic speeds or high angles of attack where flow separation occurs. Structural nonlinearities are classified as being either distributed or concentrated. In general, distributed structural nonlinearities are governed by elastodynamic deformations that affect the whole structure. On the other hand, concentrated nonlinearities act locally and commonly arise from worn hinges of the control surfaces, loose control linkages, or are related to material behavior. A comprehensive review on this subject has been presented by Lee

*Corresponding author. Tel.: +98 21 88011001 × 3391; fax: +98 21 88006544.
E-mail address: ghadirib@modares.ac.ir (B. Ghadiri).

0889-9746/$ - see front matter © 2006 Elsevier Ltd. All rights reserved.
doi:10.1016/j.jfluidstructs.2006.10.010

Nomenclature

a_h	nondimensional distance from wing section mid-chord to elastic axis
b	wing section semi-chord
c	chord
C_h, C_α	damping coefficients in plunge and pitch
D	damping energy
dC_L	wing elemental aerodynamic lift coefficient
dC_M	wing elemental pitching moment coefficient
dof	degree of freedom
EI	bending stiffness
$f_h(\eta)$	first plunge mode shape function
$f_\alpha(\eta)$	first pitch mode shape function
h	plunge displacement
h_1, α_1	time-dependent part of plunge and pitch motions
HB	harmonic balance method
$I_{C.G}$	mass moment of inertia about center of gravity
I_α	mass moment of inertia about elastic axis
$G(\xi_1)$	structural nonlinearity in plunge
GJ	torsional stiffness
K_1, K_2	constants of mode shape functions
l	span length of wing
L	wing aerodynamic lift force
LCO	limit cycle oscillations
m	wing mass per unit length
$M(\alpha_1)$	structural nonlinearity in pitch
$M_{E.A}$	wing pitching moment about elastic axis
Q_h, Q_α	generalized forces corresponding to plunge and pitch
r_α	radius of gyration about elastic axis
T	kinetic energy
t	time
U	free-stream velocity
U^*	nondimensional velocity
U_L^*	nondimensional linear flutter speed
V	potential energy
δW	virtual work
x_α	nondimensional distance from elastic axis to center of mass
y	coordinate along wing span
α	pitch angle of wing section
$\beta_\alpha, \beta_{\alpha^3}$	constants in nonlinear term $M(\alpha_1)$
β_ξ, β_{ξ^3}	constants in nonlinear term $G(\xi_1)$
β_1, β_2	constants in mode shape functions
$\varepsilon_1, \varepsilon_2$	constants in Wagner's function
ζ_ξ, ζ_α	viscous damping ratios in plunge and pitch
η	dimensionless coordinate along the wing span
μ	wing/air mass ratio
ξ	nondimensional plunge displacement
ξ_1	nondimensional time-dependent part of plunge motion
ρ	air density
τ	nondimensional time
$\phi(\tau)$	Wagner's function
ψ_1, ψ_2	constants in Wagner's function
ω	frequency of limit cycle oscillations
ω_h, ω_α	natural frequencies in plunge and pitch
$\bar{\omega}$	frequency ratio

et al. (1999a). These systems exhibit nonlinear dynamic response characteristics such as limit cycle oscillations (LCO). LCO can only occur in nonlinear systems; consequently, it is not possible to predict LCO using a purely linear analysis.

Cubic nonlinearity as a concentrated structural nonlinearity for a two-dof (degree-of-freedom) airfoil was first studied by Woolsten et al. (1957) and Shen (1959). For an airfoil containing a hardening cubic nonlinearity, they showed that, as the flow velocity increases beyond the linear flutter speed, the motion oscillates with limited amplitude. Lee and LeBlanc (1986), Lee et al. (1999b) analyzed a 2-dof airfoil motion with cubic nonlinearity in pitch using a time marching simulation. Price et al. (1995) studied a cubic nonlinearity in the pitch direction using the describing function method. They could predict the LCO amplitude in the pitch direction with this semi-analytical method. Liu et al. (2000) applied center manifold theory to obtain the LCO frequency of airfoils with cubic nonlinearity. Most recently, Lee et al. (2005) have used harmonic balance (HB) method in order to predict LCO frequency and amplitude of motion.

O'Neil and Strganac (1998) investigated the aeroelastic response of a rigid wing supported by a cubic nonlinear spring. They studied the dynamic response of a two-dof wing section via the quasi-steady assumption in the frequency domain. In another research, Marzocca et al. (2002) studied the aeroelastic response and flutter of a swept wing containing a cubic nonlinearity in an incompressible flow, but the prediction of LCO amplitude and frequency was not within the scope of that paper. Rather they concentrated on the flutter instability boundaries.

In the present work, the governing aeroelastic equations of a two-dof rectangular cantilever wing are derived through applying the strip theory and unsteady aerodynamics, and they are studied in the time domain. In order to apply strip theory, mode shapes of the cantilever beam are used. A linear analysis is carried out for verification. HB methods of different orders are applied in order to predict LCO amplitude and frequency of a two-dof uniform wing with hardening cubic nonlinearity and the results are compared with the exact numerical solution of the derived equations. Also,

nonlinear aeroelastic analysis of a wing containing a softening cubic nonlinearity is studied using the exact numerical solution.

2. Governing aeroelastic equations

The Lagrange equations can be used to obtain the governing aeroelastic equations of a rectangular wing in an incompressible flow. Consider a two-dof wing oscillating in pitch and plunge. The sketch of a wing section is shown in Fig. 1. As shown, the plunge deflection is denoted by h, positive downward direction, and the pitch angle α, positive nose up, respectively; b is the semi-chord length, and x_α and a_h are dimensionless distance of the elastic axis from center of mass and midchord, respectively. The notations used in the analysis of the two-dof wing are shown in Fig. 2. In addition to the illustrated notations, the length of span is denoted by l, and y is the horizontal coordinate in the span direction.

The Lagrange equations for a two-dof rectangular wing oscillating in pitch and plunge can be written as follows:

$$\frac{\mathrm{d}}{\mathrm{d}t}\left(\frac{\partial T}{\partial \dot{h}_1}\right)-\frac{\partial T}{\partial h_1}+\frac{\partial V}{\partial h_1}+\frac{\partial D}{\partial \dot{h}_1}=Q_h,\quad \frac{\mathrm{d}}{\mathrm{d}t}\left(\frac{\partial T}{\partial \dot{\alpha}_1}\right)-\frac{\partial T}{\partial \alpha_1}+\frac{\partial V}{\partial \alpha_1}+\frac{\partial D}{\partial \dot{\alpha}_1}=Q_\alpha, \tag{1}$$

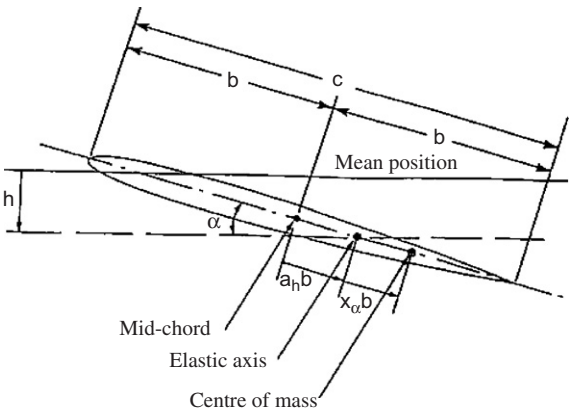

Fig. 1. Schematic figure of the wing section [from Lee et al. (1999a)].

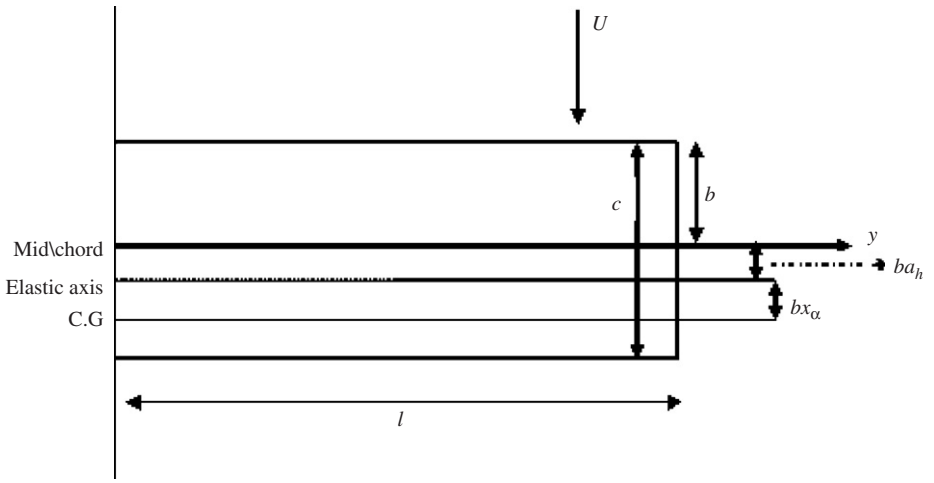

Fig. 2. Sketch of a rectangular cantilever wing.

where h_1 and α_1 are the time-dependent parts of the plunge and pitch motions. The kinetic, potential and damping energies, denoted by T, V and D, respectively, may be expressed as follows for the two-dof wing:

$$T = \frac{1}{2}\int_0^l [m(\dot{h} + bx_\alpha\dot{\alpha})^2 + I_{C.G}\dot{\alpha}^2]\,\mathrm{d}y, \quad V = \frac{1}{2}\int_0^l \left[EI\left(\frac{\partial^2 h}{\partial y^2}\right)^2 + GJ\left(\frac{\partial\alpha}{\partial y}\right)^2\right]\mathrm{d}y, \tag{2,3}$$

$$D = \frac{1}{2}\int_0^l [C_h\dot{h}^2 + C_\alpha\dot{\alpha}^2]\,\mathrm{d}y, \tag{4}$$

where $m, I_{C.G}, EI, GJ, C_h$ and C_α are wing mass per unit length, wing mass moment of inertia per unit length about wing center of gravity, bending stiffness, torsional stiffness, and the bending and torsional damping coefficients, respectively.

Assuming the rectangular wing as a uniform cantilever beam, these mode shapes can be used for plunge and pitch dof as follows (Marzocca et al., 2002):

$$F_h(\eta) = K_1\left\{\left(\frac{\sinh\beta_1 + \sin\beta_1}{\cosh\beta_1 + \cos\beta_1}\right)(\cos(\beta_1\eta) - \cosh(\beta_1\eta)) + \sinh(\beta_1\eta) - \sin(\beta_1\eta)\right\}, \tag{5}$$

$$F_\alpha(\eta) = K_2\sin(\beta_2\eta), \tag{6}$$

where $\beta_1 = 0.5969\pi$ for the first bending mode, $\beta_2 = 0.5\pi$ for the first torsional mode , η is a dimensionless coordinate along the wing span ($\eta = y/l$), and K_1 and K_2 are constants. Combining the time-dependent parts of the motion and assumed mode shapes, it can be deduced that

$$h = F_h(\eta)h_1(t), \quad \alpha = F_\alpha(\eta)\alpha_1(t). \tag{7,8}$$

Applying assumed mode shapes by inserting Eqs. (7) and (8) into Eqs. (2), (3) and (4), the following expressions can be obtained for the kinetic, potential and damping energy of the rectangular cantilever wing:

$$T = \frac{A_3}{2}(ml\dot{h}_1^2) + \frac{A_4}{2}lm(bx_\alpha\dot{\alpha}_1)^2 + A_5(lmbx_\alpha\dot{h}_1\dot{\alpha}_1) + \frac{A_4}{2}lI_{C.G}\dot{\alpha}_1^2, \tag{9}$$

$$V = \frac{A_1}{2}\left(\frac{EI}{l^3}h_1^2\right) + \frac{A_2}{2}\left(\frac{GJ}{l}\alpha_1^2\right), \tag{10}$$

$$D = l\frac{A_3}{2}C_h\dot{h}_1^2 + l\frac{A_4}{2}C_\alpha\dot{\alpha}_1^2, \tag{11}$$

where $A_1, ..., A_5$ are constants and are given in Appendix A. Inserting Eqs. (9)–(11) in Eq. (1), we can write

$$A_3(lm\ddot{h}_1) + A_5(lmbx_\alpha\ddot{\alpha}_1) + A_3lC_h\dot{h}_1 + A_1\left(\frac{EI}{l^3}h_1\right) = Q_h, \tag{12}$$

$$A_4lm(bx_\alpha)^2\ddot{\alpha}_1 + A_5(lmbx_\alpha\ddot{h}_1) + lA_4I_{C.G}\ddot{\alpha}_1 + lA_4C_\alpha\dot{\alpha}_1 + A_2\left(\frac{GJ}{l}\alpha_1\right) = Q_\alpha. \tag{13}$$

Defining

$$\xi = \frac{h}{b}, \quad r_\alpha = \sqrt{\frac{I_\alpha}{mb^2}}, \quad \mu = \frac{m}{\pi\rho b^2}, \quad U^* = \frac{U}{b\omega_\alpha}, \quad \omega_h = \sqrt{\frac{A_1EI}{A_3ml^4}}, \quad \omega_\alpha = \sqrt{\frac{A_2GJ}{A_4I_\alpha l^2}}, \quad \bar{\omega} = \frac{\omega_h}{\omega_\alpha},$$

$$\zeta_\xi = \frac{1}{2}\sqrt{\frac{A_3}{A_1}}\frac{l^2C_h}{\sqrt{mEI}}, \quad \zeta_\alpha = \frac{1}{2}\sqrt{\frac{A_4}{A_2}}\frac{C_\alpha l}{\sqrt{I_\alpha GJ}}.$$

Eqs. (12) and (13) can be written as

$$A_3\xi_1'' + A_5(x_\alpha\alpha_1'') + 2A_3\zeta_\xi\frac{\bar{\omega}}{U^*}\xi_1' + A_3\left(\frac{\bar{\omega}}{U^*}\right)^2\xi_1 = \frac{b}{mU^2l}Q_h, \tag{14}$$

$$A_5\left(\frac{x_\alpha}{r_\alpha^2}\xi_1''\right) + A_4\alpha_1'' + 2A_4\frac{\zeta_\alpha}{U^*}\alpha_1' + A_4\left(\frac{1}{U^*}\right)^2\alpha_1 = \frac{b^2}{I_\alpha U^2 l}Q_\alpha, \tag{15}$$

where ξ is a dimensionless plunge displacement, ω_h and ω_α are natural frequencies of uncoupled plunging and pitching modes, ζ_ξ and ζ_α are the viscous damping ratios in plunge and pitch, and the prime sign denotes differentiation with respect to the nondimensional time τ defined as $\tau = Ut/b$. Also U^*, $\bar{\omega}$ and r_α are nondimensional speed, frequency ratio and radius of gyration about the elastic axis, respectively.

By extending Eqs. (14) and (15) to nonlinear form, concentrated structural nonlinearities can be analyzed. In this case, these equations can be written as a system of nonlinear ordinary differential equations (ODEs) as follows:

$$A_3\xi_1'' + A_5(x_\alpha\alpha_1'') + 2A_3\zeta_\xi\frac{\bar{\omega}}{U^*}\xi_1' + A_3\left(\frac{\bar{\omega}}{U^*}\right)^2 G(\xi_1) = \frac{b}{mU^2l}Q_h, \tag{16}$$

$$A_5\left(\frac{x_\alpha}{r_\alpha^2}\xi_1''\right) + A_4\alpha_1'' + 2A_4\frac{\zeta_\alpha}{U^*}\alpha_1' + A_4\left(\frac{1}{U^*}\right)^2 M(\alpha_1) = \frac{b^2}{I_\alpha U^2 l}Q_\alpha, \tag{17}$$

where $G(\xi_1)$ and $M(\alpha_1)$ are nonlinear stiffness terms which are defined for a cubic nonlinearity as

$$G(\xi_1) = \beta_\xi\xi_1 + \beta_{\xi^3}\xi_1^3, \quad M(\alpha_1) = \beta_\alpha\alpha_1 + \beta_{\alpha^3}\alpha_1^3. \tag{18,19}$$

Terms Q_h and Q_α in Eqs. (16) and (17) are the generalized forces corresponding to the generalized coordinates h_1 and α_1, respectively. These terms are obtained using the virtual work law and they are related to the lift and pitching moment coefficients about the elastic axis. Ignoring the thickness of the airfoil, the following expressions for the lift and pitching moment of an airfoil in an incompressible flow were given by Fung (1969):

$$\begin{aligned} dC_L(\tau) &= \pi(\xi'' - a_h\alpha'' + \alpha') + 2\pi\left(\alpha(0) + \xi'(0) + \left[\frac{1}{2} - a_h\right]\alpha'(0)\right)\phi(\tau) \\ &\quad + 2\pi\int_0^\tau \phi(\tau-\sigma)\left[\alpha'(\sigma) + \xi''(\sigma) + \left(\frac{1}{2} - a_h\right)\alpha''(\sigma)\right]\mathrm{d}\sigma, \end{aligned}$$

$$\begin{aligned} dC_M(\tau) &= \pi\left(\frac{1}{2} + a_h\right)\left\{\alpha(0) + \xi'(0) + \left[\frac{1}{2} - a_h\right]\alpha'(0)\right\}\phi(\tau) \\ &\quad + \pi\left(\frac{1}{2} + a_h\right)\int_0^\tau \phi(\tau-\sigma)\left\{\alpha'(\sigma) + \xi''(\sigma) + \left(\frac{1}{2} - a_h\right)\alpha''(\sigma)\right\}\mathrm{d}\sigma \\ &\quad + \frac{\pi}{2}a_h(\xi'' - a_h\alpha'') - \left(\frac{1}{2} - a_h\right)\frac{\pi}{2}\alpha' - \frac{\pi}{16}\alpha'', \end{aligned} \tag{20}$$

where Wagner's function $\phi(\tau)$ is given by

$$\phi(\tau) = 1 - \psi_1 e^{-\varepsilon_1\tau} - \psi_2 e^{-\varepsilon_2\tau}, \tag{21}$$

and the constants $\psi_1 = 0.165$, $\psi_2 = 0.335$, $\varepsilon_1 = 0.0455$ and $\varepsilon_2 = 0.3$ are obtained from Lee et al. (1999a).

In order to apply these expressions for the wing, strip theory is used. In this approximation, the known results for two-dimensional flow (infinite span airfoil) are employed in order to calculate the aerodynamic forces on a lifting surface of finite span (Dowell et al., 2004). Eq. (20) gives the lift and pitching moment coefficients of an airfoil which can be interpreted as an element of the wing. In this theory, these expressions are integrated to obtain the overall lift and pitching moment about the elastic axis for the wing. So, according to strip theory, the virtual work δW done on the wing by these aerodynamic forces as the wing moves through the virtual displacements δh and $\delta\alpha$, can be written as

$$\delta W = -\left[\rho U^2 bl\int_0^1 dC_L f_h(\eta)\,\mathrm{d}\eta\right]\delta h_1 + \left[2\rho U^2 b^2 l\int_0^1 dC_M f_\alpha(\eta)\,\mathrm{d}\eta\right]\delta\alpha_1, \tag{22}$$

and as a result, terms Q_h and Q_α are derived using following formulas:

$$Q_h = -\rho U^2 bl\int_0^1 dC_L f_h(\eta)\,\mathrm{d}\eta, \quad Q_\alpha = 2\rho U^2 b^2 l\int_0^1 dC_M f_\alpha(\eta)\,\mathrm{d}\eta, \tag{23,24}$$

in which dC_L and dC_M are the lift and pitching moment coefficients of an element of the wing given in Eq. (20). Final expressions for terms Q_h and Q_α are obtained using the assumed structural modes in Eqs. (23) and (24). These modes

are given in Eqs. (5) and (6). Thus, by inserting Eqs. (5)–(8) in Eqs. (23) and (24), the generalized forces can be expressed as follows:

$$\begin{aligned} Q_h = & -\rho U^2 bl\left[\pi(A_3\xi_1'' - A_5 a_h\alpha_1'' + A_5\alpha_1') + 2\pi\left(A_5\alpha_1(0) + A_3\xi_1'(0) + \left[\frac{1}{2} - a_h\right]A_5\alpha_1'(0)\right)\phi(\tau)\right. \\ & \left. + 2\pi\int_0^\tau \phi(\tau-\sigma)\left[A_5\alpha_1'(\sigma) + A_3\xi_1''(\sigma) + \left(\frac{1}{2} - a_h\right)A_5\alpha_1''(\sigma)\right]\mathrm{d}\sigma\right], \end{aligned}$$

$$\begin{aligned} Q_\alpha = & 2\rho U^2 b^2 l\left[\pi\left(\frac{1}{2} + a_h\right)\left\{A_4\alpha_1(0) + A_5\xi_1'(0) + \left[\frac{1}{2} - a_h\right]A_4\alpha_1'(0)\right\}\phi(\tau)\right. \\ & + \pi\left(\frac{1}{2} + a_h\right)\int_0^\tau \phi(\tau-\sigma)\left\{A_4\alpha_1'(\sigma) + A_5\xi_1''(\sigma) + \left(\frac{1}{2} - a_h\right)A_4\alpha_1''(\sigma)\right\}\mathrm{d}\sigma \\ & \left. + \frac{\pi}{2}a_h(A_5\xi_1'' - A_4 a_h\alpha_1'') - \left(\frac{1}{2} - a_h\right)\frac{\pi}{2}A_4\alpha_1' - \frac{\pi}{16}A_4\alpha_1''\right]. \end{aligned} \tag{25}$$

By utilizing Eq. (25) in Eqs. (16) and (17), the governing aeroelastic equations for the rectangular cantilever wing can be obtained. But, due to the existence of the integro-differential terms in Eq. (25), it is very difficult to integrate them numerically. By using four new variables, first introduced by Lee et al. (1997),

$$w_1 = \int_0^\tau \mathrm{e}^{-\varepsilon_1(\tau-\sigma)}\alpha_1(\sigma)\,\mathrm{d}\sigma, \quad w_2 = \int_0^\tau \mathrm{e}^{-\varepsilon_2(\tau-\sigma)}\alpha_1(\sigma)\,\mathrm{d}\sigma,$$

$$w_3 = \int_0^\tau \mathrm{e}^{-\varepsilon_1(\tau-\sigma)}\xi_1(\sigma)\,\mathrm{d}\sigma, \quad w_4 = \int_0^\tau \mathrm{e}^{-\varepsilon_2(\tau-\sigma)}\xi_1(\sigma)\,\mathrm{d}\sigma, \tag{26}$$

in Eq. (25) and eventually in Eqs. (16) and (17), the governing aeroelastic equations for a rectangular cantilever wing can be written as follows:

$$c_0\xi_1'' + c_1\alpha_1'' + c_2\xi_1' + c_3\alpha_1' + c_4\xi_1 + c_5\alpha_1 + c_6 w_1 + c_7 w_2 + c_8 w_3 + c_9 w_4 + A_3\left(\frac{\bar{\omega}}{U^*}\right)^2 G(\xi_1) = f(\tau), \tag{27}$$

$$d_0\xi_1'' + d_1\alpha_1'' + d_2\alpha_1' + d_3\alpha_1 + d_4\xi_1' + d_5\xi_1 + d_6 w_1 + d_7 w_2 + d_8 w_3 + d_9 w_4 + A_4\left(\frac{1}{U^*}\right)^2 M(\alpha_1) = g(\tau). \tag{28}$$

The coefficients $c_0, c_1, ..., c_9$, $d_0, d_1, ..., d_9$ and expressions $f(\tau)$ and $g(\tau)$ are given in Appendix B.

3. Numerical solution

The governing aeroelastic equations in the time domain, Eqs. (27) and (28), can easily be rewritten as a set of first-order ODEs. By a suitable transformation, the resulting set of eight ODEs is given as follows:

$$\frac{\mathrm{d}X}{\mathrm{d}\tau} = F(x,\tau), \tag{29}$$

where

$$X = [x_1 \quad x_2 \quad x_3 \quad x_4 \quad x_5 \quad x_6 \quad x_7 \quad x_8]^{\mathrm{T}} = [\alpha_1 \quad \alpha_1' \quad \xi_1 \quad \xi_1' \quad w_1 \quad w_2 \quad w_3 \quad w_4]^{\mathrm{T}}. \tag{30}$$

The standard fourth-order Runge–Kutta method can be used to integrate the system of Eq. (29) for given initial conditions. It can be deduced easily from Eq. (26) that

$$\tau = 0 \Rightarrow w_1 = w_2 = w_3 = w_4 = 0. \tag{31}$$

So, the initial conditions of the system can be expressed as

$$\begin{aligned} X(0) &= [x_1(0) \quad x_2(0) \quad x_3(0) \quad x_4(0) \quad x_5(0) \quad x_6(0) \quad x_7(0) \quad x_8(0)]^{\mathrm{T}} \\ &= [\alpha_1(0) \quad \alpha_1'(0) \quad \xi_1(0) \quad \xi_1'(0) \quad 0 \quad 0 \quad 0 \quad 0]^{\mathrm{T}}, \end{aligned} \tag{32}$$

where $\alpha_1(0), \alpha_1'(0), \xi_1(0)$ and $\xi_1'(0)$ are the initial values of the time-dependent part of pitch displacement, pitch velocity, plunge displacement and plunge velocity, respectively. The accuracy of the scheme at each time step is $\mathcal{O}(\Delta\tau^5)$.

Finally, for a selected section of the wing which is defined by $\eta \in [0, 1]$ (from root to tip of the wing) at a specific time, pitch and plunge displacements can be obtained by combining assumed mode shapes and time-dependent parts as follows:

$$\alpha(\tau, \eta) = \alpha_1(\tau) f_\alpha(\eta), \quad \xi(\tau, \eta) = \xi_1(\tau) f_h(\eta). \tag{33}$$

4. Harmonic balance method

The HB method is an efficient method for the prediction of the frequency and amplitude of LCO which occurs at speeds above the linear flutter speed for wings containing a hardening cubic nonlinearity. This method gives the harmonic solution of a system of nonlinear differential equations, the amplitude and frequency of which is constant and similar to LCO conditions. In order to apply this method, plunge and pitch motions should be assumed as a trigonometric series, such as Fourier series. So, the time-dependent part of plunge and pitch motions can be approximated as follows:

$$\alpha_1(\tau) = a_1 \sin(\omega\tau) + \sum_{i=3,5,7,9,\ldots} a_i \sin(i\omega\tau) + b_i \cos(i\omega\tau), \tag{34}$$

$$\xi_1(\tau) = \sum_{j=1,3,5,9,\ldots..} e_j \sin(j\omega\tau) + f_j \cos(j\omega\tau). \tag{35}$$

Similar to the feature assumed for LCO, coefficients a_i, b_i, e_j, f_j and also the LCO frequency ω are constant with respect to dimensionless time τ. Substituting Eqs. (34) and (35) in Eqs. (27) and (28) and ignoring the terms which are dependent on initial conditions, a system of trigonometric equations is obtained. Collecting the coefficients of $\sin(i\omega\tau)$ and $\cos(i\omega\tau)$ $(i = 1, 3, 5, \ldots)$, we obtain a system of algebraic equations with $\omega, a_1, a_i, b_i, e_j$ and f_j $(i = 3, 5, 7, \ldots; j = 3, 5, 7, \ldots)$ as variables. The maximum values of the indices i and j are equal. The order of the harmonic balance method is also equal to this maximum value.

For instance, for the first-order HB method (HB1) $(i = j = 1)$, the nonlinear terms $\alpha_1^3(\tau)$ and $\xi_1^3(\tau)$ can be expressed as Eqs. (36) and (37) and higher harmonics in $3\omega\tau$ and above are ignored:

$$\alpha_1^3(\tau) = \tfrac{3}{4} a_1^3 \sin(\omega\tau), \tag{36}$$

$$\xi_1^3(\tau) = \tfrac{3}{4} e_1^3 \sin(\omega\tau) + \tfrac{3}{4} e_1^2 f_1 \cos(\omega\tau) + \tfrac{3}{4} e_1 f_1^2 \sin(\omega\tau) + \tfrac{3}{4} f_1^3 \cos(\omega\tau). \tag{37}$$

Table 1
Case studies of the linear analysis: physical and geometrical characteristics

Case	NACA wing section	$\omega_h s$ (rad/s)	ω_α (rad/s)	b (m)	l (m)
30A	16-010	23.8π	166π	0.0509	0.6299
30B	16-010	24π	176π	0.0509	0.6299
40C	16-010	18π	116.4π	0.0509	0.6299
91-2	16-010	11π	86π	0.1015	1.2192
91-3	16-010	10π	80π	0.1015	1.2192

Table 2
Case studies of the linear analysis: nondimensional characteristics

Case	NACA wing section	x_α	a_h	r_α^2	μ
30A	16-010	0.220	−0.300	0.311	36.8
30B	16-010	0.120	−0.200	0.277	37.8
40C	16-010	0.150	−0.230	0.287	8.74
91-2	16-010	−0.056	−0.124	0.179	41.7
91-3	16-010	0.012	−0.032	0.160	44.3

By utilizing Eqs. (34) and (35) for $i=j=1$ and also Eqs. (36) and (37), the resulting set of nonlinear algebraic equations for the first-order HB method can be obtained as follows:

$$-c_0e_1\omega^2-c_1a_1\omega^2-c_2f_1\omega+c_4e_1+c_5a_1+\frac{c_6a_1\varepsilon_1}{\varepsilon_1^2+\omega^2}+\frac{c_7a_1\varepsilon_2}{\varepsilon_2^2+\omega^2}+\frac{c_8e_1\varepsilon_1}{\varepsilon_1^2+\omega^2}+\frac{c_8f_1\omega}{\varepsilon_1^2+\omega^2}$$
$$+\frac{c_9e_1\varepsilon_2}{\varepsilon_2^2+\omega^2}+\frac{c_9f_1\omega}{\varepsilon_2^2+\omega^2}+A_3\left(\frac{\bar{\omega}}{U^*}\right)^2\left[\beta_\xi e_1+\frac{3}{4}\beta_{\xi^3}(e_1^3+e_1f_1^2)\right]=0, \tag{38}$$

$$-c_0f_1\omega^2+c_2e_1\omega+c_3a_1\omega+c_4f_1-\frac{c_6a_1\omega}{\varepsilon_1^2+\omega^2}-\frac{c_7a_1\omega}{\varepsilon_2^2+\omega^2}-\frac{c_8e_1\omega}{\varepsilon_1^2+\omega^2}+\frac{c_8f_1\varepsilon_1}{\varepsilon_1^2+\omega^2}$$
$$-\frac{c_9e_1\omega}{\varepsilon_2^2+\omega^2}+\frac{c_9f_1\varepsilon_2}{\varepsilon_2^2+\omega^2}+A_3\left(\frac{\bar{\omega}}{U^*}\right)^2\left[\beta_\xi f_1+\frac{3}{4}\beta_{\xi^3}(f_1^3+f_1e_1^2)\right]=0, \tag{39}$$

$$-d_0e_1\omega^2-d_1a_1\omega^2+d_3a_1-d_4f_1\omega+d_5e_1+\frac{d_6a_1\varepsilon_1}{\varepsilon_1^2+\omega^2}+\frac{d_7a_1\varepsilon_2}{\varepsilon_2^2+\omega^2}+\frac{d_8e_1\varepsilon_1}{\varepsilon_1^2+\omega^2}+\frac{d_8f_1\omega}{\varepsilon_1^2+\omega^2}$$
$$+\frac{d_9e_1\varepsilon_2}{\varepsilon_2^2+\omega^2}+\frac{d_9f_1\omega}{\varepsilon_2^2+\omega^2}+A_4\left(\frac{1}{U^*}\right)^2\left[\beta_\alpha a_1+\frac{3}{4}\beta_{\alpha^3}a_1^3\right]=0, \tag{40}$$

$$-d_0f_1\omega^2+d_2a_1\omega+d_4e_1\omega+d_5f_1-\frac{d_6a_1\omega}{\varepsilon_1^2+\omega^2}-\frac{d_7a_1\omega}{\varepsilon_2^2+\omega^2}-\frac{d_8e_1\omega}{\varepsilon_1^2+\omega^2}+\frac{d_8f_1\varepsilon_1}{\varepsilon_1^2+\omega^2}$$
$$-\frac{d_9e_1\omega}{\varepsilon_2^2+\omega^2}+\frac{d_9f_1\varepsilon_2}{\varepsilon_2^2+\omega^2}=0. \tag{41}$$

As can be seen, the number of equations for HB1 is 4. For every increment in the order of this method, four new unknown variables and therefore four other nonlinear algebraic equations will be added to the previous number. Therefore, by increasing the order of the HB method, our resulting system of algebraic nonlinear equations will be more complex. However, more accurate results can be obtained by increasing the order of this method. For the sake of brevity, the resulting sets of nonlinear HB equations for higher orders are not given in this paper, but the results obtained up to fifth order are discussed.

Solving the resulting system of equations such as Eqs. (38)–(41) for HB1, the LCO frequency and amplitude can easily be obtained by using the Newton method for a set of nonlinear algebraic equations. Having found the time-dependent part of pitch and plunge motions, the LCO pitch and plunge amplitude will be obtained through Eq. (33).

Table 3
Calculated and experimental results for flutter speed

Case	Experimental flutter speed (m/s)	Calculated flutter speed (m/s)	Error (percentage)
30A	103.713	94.438	−8.94
30B	102.372	95.731	−6.49
40C	33.662	33.546	−0.34
91-2	92.984	86.406	−7.07
91-3	71.079	70.209	−1.22

Table 4
Case studies of the nonlinear analysis

Case	β_α	β_α^3	β_ξ	β_ξ^3	U_L^*
1	1	3	1	0	6.52269
2	1	5	1	1	6.52269
3	1	−3	1	0	6.52269

5. Linear analysis

Linear aeroelastic analysis of the rectangular cantilever wing was carried out in order to verify the derived formulations. For this reason, experimental data for the flutter speed of the uniform cantilever wing of Barmby et al. (1950) are used. The physical characteristics of the tested wings and their nondimensional parameters are presented in Tables 1 and 2, respectively. In order to find the flutter boundaries of these case studies, linear analysis was carried out via inserting ξ_1 and α_1 instead of the nonlinear terms $G(\xi_1)$ and $M(\alpha_1)$ in Eqs. (27) and (28), respectively. The standard fourth-order Runge–Kutta method was applied to obtain exact numerical solutions for the resulting set of first-order differential equations. As a result, pitch and plunge displacements of the wing versus nondimensional time for the desired section of the wing which is defined by η can be plotted.

The study of dynamical response of the wing at different velocities shows whether it decays to zero or diverges, and the linear flutter speed is calculated for each case. Experimental and calculated flutter speeds for five different cases are given in Table 3. It can be seen that this formulation provides good agreement with the experimental data, and the error of our proposed method compared to the experimental data in all five cases is below 10%.

In the strip theory approximation, the chordwise pressure distribution at any spanwise station is assumed to depend only on the downwash at that station given by the two-dimensional aerodynamic theory and to be independent of the downwash at any other spanwise station (Dowell et al., 2004). Actually, this assumption causes an error in our

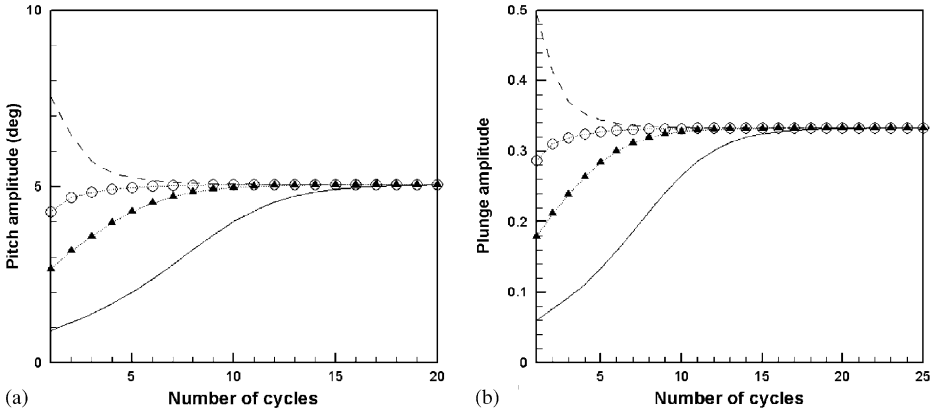

Fig. 3. Wing tip variation of amplitude with number of cycles for Case 1 and $U^* = 1.01U_L^*$: (a) amplitude of pitch motion; (b) amplitude of plunge motion; — —, $\alpha_1(0) = 1°$; ...▲...., $\alpha_1(0) = 3°$; ··◯···, $\alpha_1(0) = 5°$; – – – –, $\alpha_1(0) = 10°$.

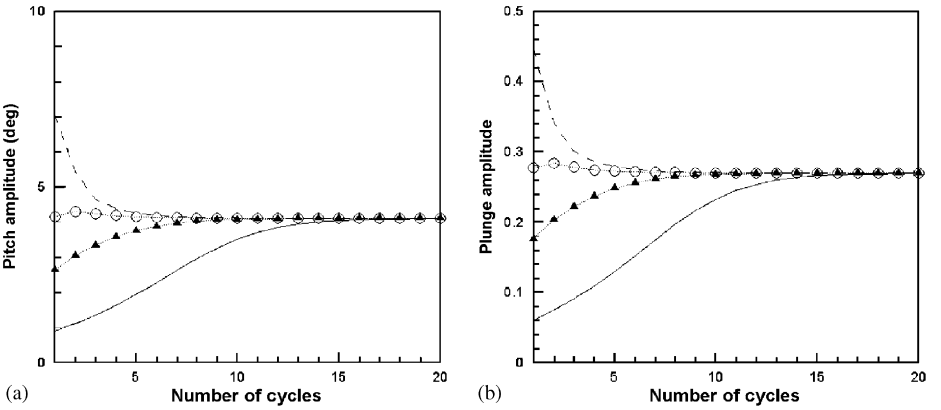

Fig. 4. Wing tip variation of amplitude with number of cycles for Case 2 and $U^* = 1.01U_L^*$: (a) amplitude of pitch motion; (b) amplitude of plunge motion; — —, $\alpha_1(0) = 1°$; ...▲...., $\alpha_1(0) = 3°$; ··◯···, $\alpha_1(0) = 5°$; – – – –, $\alpha_1(0) = 10°$.

calculations and it is the main reason of the difference between experimental and calculated data for the flutter speed. However, by our comparison, it is shown that this error can be ignored. The assumption of two-dimensional flow and also the use of only the first mode shape of a cantilever beam can be other sources of error.

6. Nonlinear analysis

Nonlinear aeroelastic analysis of rectangular cantilever wings containing softening and hardening cubic nonlinearities was undertaken for three different cases given in Table 4. By considering the nonlinearities, it is possible to investigate the dynamical response of the aeroelastic systems beyond the linear flutter boundary. Nonlinear aeroelastic analysis not only describes phenomena such as LCO, but also in the case of softening nonlinearity, it can predict the nonlinear flutter boundary which may be below the linear one due to the effect of initial conditions.

The problem of LCO of a rectangular cantilever wing with a hardening cubic nonlinearity was investigated via the exact numerical solution of the system of Eqs. (27) and (28) and the HB method. Two cases were considered, with the different hardening cubic restoring forces. The nonlinear terms $G(\xi_1)$ and $M(\alpha_1)$ for Cases 1 and 2 are given in Table 4. Also, the following dimensionless numerical values are used for the wings geometry and characteristics:

$$a_h = -0.5, \quad \mu = 100.0, \quad \zeta_\xi = \zeta_\alpha = 0, \quad x_\alpha = 0.25, \quad r_\alpha = 0.5, \quad \bar{\omega} = 0.2.$$

In the first case, the wing containing a hardening cubic nonlinearity only in the pitch dof was considered, but in the second case the dynamical response of the wing with this nonlinearity in both dofs was investigated. The nondimensional linear flutter speed of $U_L^* = 6.52269$ is obtained by using the standard fourth-order Runge–Kutta method, which was already discussed.

LCO is the phenomenon which occurs at speeds higher than the linear flutter speed for airfoils containing a hardening cubic nonlinearity. Due to the similarity of the aeroelastic governing equations of airfoils and rectangular cantilever

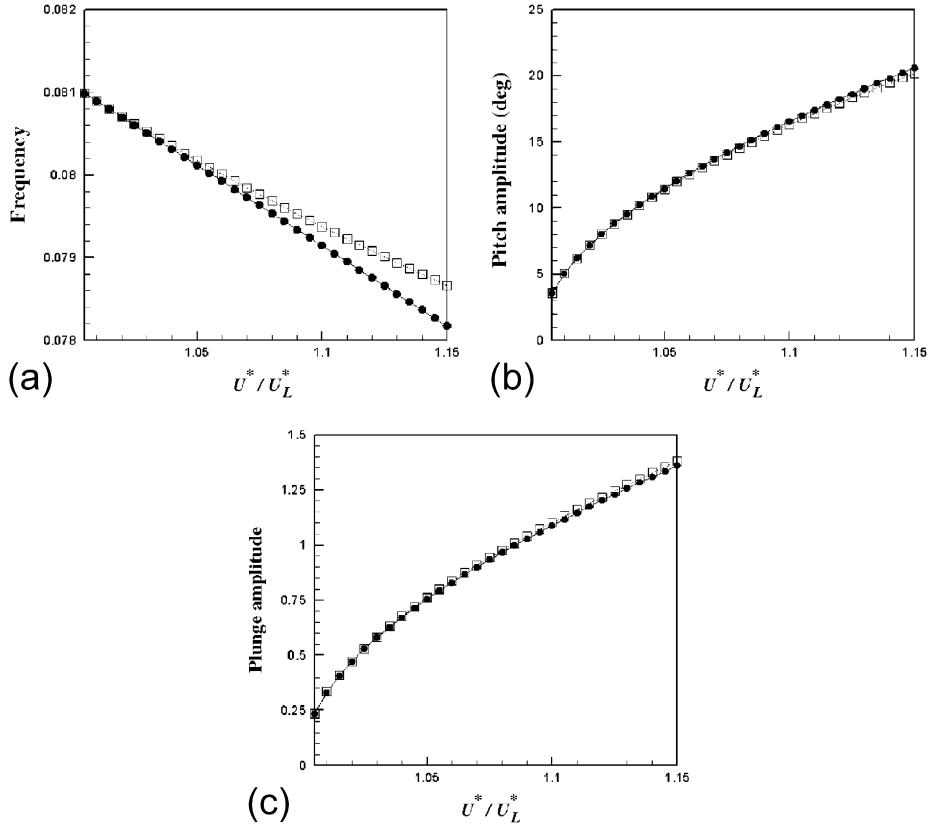

Fig. 5. Wing tip dynamical response for Case 1: (a) frequency; (b) amplitude of pitch motion; (c) amplitude of plunge motion; — —, numerical result; ···□···, HB1; ●, HB3.

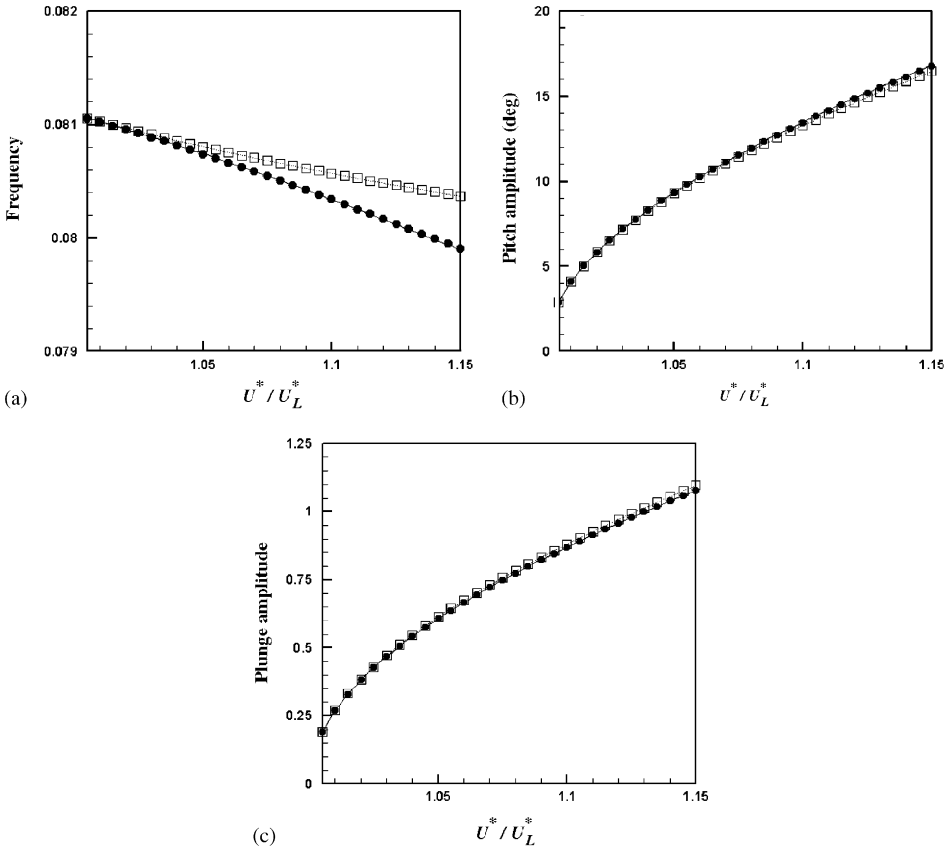

Fig. 6. Wing tip dynamical response for Case 2: (a) frequency; (b) amplitude of pitch motion; (c) amplitude of plunge motion; —, numerical result; ···□···, HB1; ●, HB3.

Table 5
LCO pitch amplitude (deg) at semi-span of the wing ($\eta = 0.5$) for Case 1; comparison between the HB methods and exact numerical solution

$\frac{U^*}{U_L^*}$	First-order harmonic balance method (HB1)	Third-order harmonic balance method (HB3)	Fifth-order harmonic balance method (HB5)	Fourth-order Runge–Kutta method
1.005	2.522232	2.524287	2.524297	2.524312
1.010	3.571113	3.576886	3.576931	3.576923
1.015	4.378790	4.389325	4.389444	4.389436
1.020	5.062076	5.078188	5.078428	5.078421
1.025	5.666139	5.688522	5.688939	5.688935
1.030	6.214167	6.243382	6.244035	6.244025
1.035	6.719847	6.756411	6.757369	6.757362
1.040	7.192146	7.236499	7.237828	7.237833
1.045	7.637241	7.689807	7.691580	7.691588
1.050	8.059646	8.120789	8.123081	8.123101
1.055	8.462760	8.532813	8.535709	8.535744
1.060	8.849215	8.928499	8.932076	8.932127
1.065	9.221118	9.309910	9.314252	9.314321
1.070	9.580152	9.678707	9.683908	9.684000
1.075	9.927723	10.036279	10.042418	10.042542
1.080	10.264992	10.383763	10.390935	10.391098
1.085	10.592948	10.722136	10.730430	10.730633

Table 5 (*continued*)

$\frac{U^*}{U_L^*}$	First-order harmonic balance method (HB1)	Third-order harmonic balance method (HB3)	Fifth-order harmonic balance method (HB5)	Fourth-order Runge–Kutta method
1.090	10.912440	11.052207	11.061735	11.061981
1.095	11.224168	11.374707	11.385530	11.385846
1.100	11.528789	11.690238	11.702471	11.702847
1.105	11.826828	11.999338	12.013071	12.013524
1.110	12.118785	12.302480	12.317818	12.318352
1.115	12.405079	12.600079	12.617122	12.617752
1.120	12.686111	12.892533	12.911359	12.912097
1.125	12.962215	13.180167	13.200876	13.201724
1.130	13.233695	13.463263	13.485953	13.486929
1.135	13.500811	13.742102	13.766851	13.767986
1.140	13.763876	14.016918	14.043890	14.045143
1.145	14.023059	14.287958	14.317220	14.318621
1.150	14.278636	14.555414	14.587037	14.588624

Table 6
LCO plunge amplitude at semi-span of the wing ($\eta = 0.5$) for Case 1; comparison between the HB methods and exact numerical solution

$\frac{U^*}{U_L^*}$	First-order harmonic balance method (HB1)	Third-order harmonic balance method (HB3)	Fifth-order harmonic balance method (HB5)	Fourth-order Runge–Kutta method
1.005	0.079811	0.079736	0.079736	0.079736
1.010	0.113169	0.112960	0.112960	0.112960
1.015	0.138967	0.138591	0.138591	0.138591
1.020	0.160885	0.160317	0.160316	0.160316
1.025	0.180341	0.179563	0.179562	0.179562
1.030	0.198063	0.197060	0.197058	0.197058
1.035	0.214479	0.213240	0.213238	0.213238
1.040	0.229870	0.228386	0.228383	0.228383
1.045	0.244429	0.242694	0.242690	0.242690
1.050	0.258295	0.256306	0.256300	0.256300
1.055	0.271575	0.269329	0.269321	0.269322
1.060	0.284350	0.281846	0.281837	0.281836
1.065	0.296686	0.293925	0.293913	0.293912
1.070	0.308634	0.305617	0.305603	0.305602
1.075	0.320237	0.316968	0.316951	0.316950
1.080	0.331532	0.328015	0.327995	0.327994
1.085	0.342549	0.338788	0.338765	0.338763
1.090	0.353313	0.349315	0.349288	0.349287
1.095	0.363847	0.359618	0.359587	0.359586
1.100	0.374169	0.369717	0.369683	0.369681
1.105	0.384297	0.379630	0.379592	0.379590
1.110	0.394245	0.389372	0.389331	0.389328
1.115	0.404026	0.398957	0.398912	0.398909
1.120	0.413653	0.408397	0.408348	0.408346
1.125	0.423134	0.417704	0.417650	0.417648
1.130	0.432480	0.426886	0.426829	0.426826
1.135	0.441698	0.435953	0.435893	0.435889
1.140	0.450798	0.444913	0.444849	0.444846
1.145	0.459784	0.453773	0.453707	0.453702
1.150	0.468665	0.462540	0.462470	0.462466

wings in an incompressible flow, the same behavior is seen for the rectangular cantilever wing by increasing the speed beyond the linear flutter speed of the wing.

LCO amplitude and frequency are independent of initial conditions. In Figs. 3 and 4, the effects of initial pitch displacement on the pitch and plunge amplitude of LCO are shown. Setting $\alpha_1'(0) = \xi_1(0) = \xi_1'(0) = 0$ and varying the time-dependent part of the initial pitch displacement $\alpha_1(0)$, the diagram of LCO pitch and plunge amplitudes versus the number of cycles can be plotted. Four different initial conditions in both cases were tested. The results show the independence of amplitude and frequency of LCO on initial conditions. As two examples, this conclusion is shown for LCO pitch and plunge amplitude for Cases 1 and 2 given in Table 4, $U^* = 1.01U_L^*$ and wing tip ($\eta = 1$).

LCO pitch and plunge amplitudes and also LCO frequency were investigated by the use of the semi-analytical method (HB method) and the exact numerical solution (standard fourth-order Runge–Kutta method) for Cases 1 and 2 given in Table 4. The results are presented in Figs. 5 and 6 for nondimensional speeds from $U^* = 1.005U_L^*$ to $U^* = 1.15U_L^*$ and for the wing tip ($\eta = 1$). In these figures, the results for the first- and third-order HB methods were compared with numerical results at the wing tip. As can be seen, there is a good agreement between the HB method and the exact numerical results, and also it is clear that the accuracy of HB method increases by increasing the order of this method. This deduction is confirmed by the results at mid-span of the wing which are presented in Tables 5 and 6.

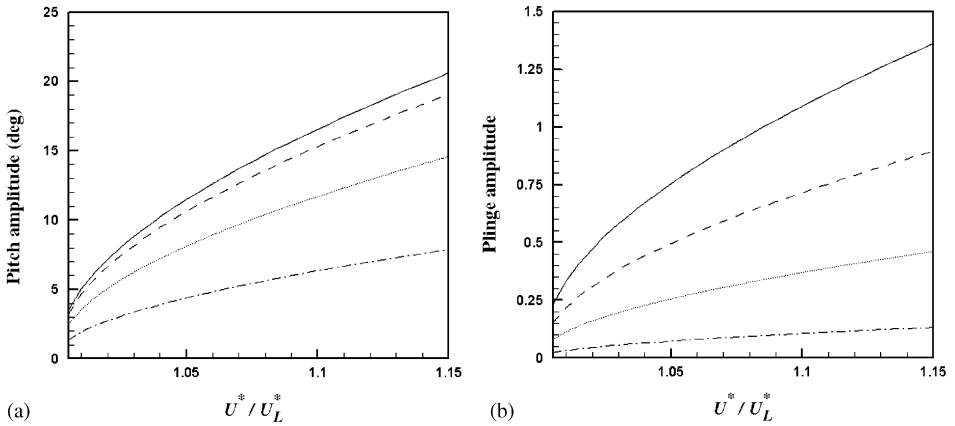

Fig. 7. Dynamical response of different section of the rectangular cantilever wing for Case 1: (a) amplitude of pitch motion; (b) amplitude of plunge motion; – - – -, $\eta = 0.25$; ……, $\eta = 0.5$; – – – , $\eta = 0.75$; —, $\eta = 1.0$.

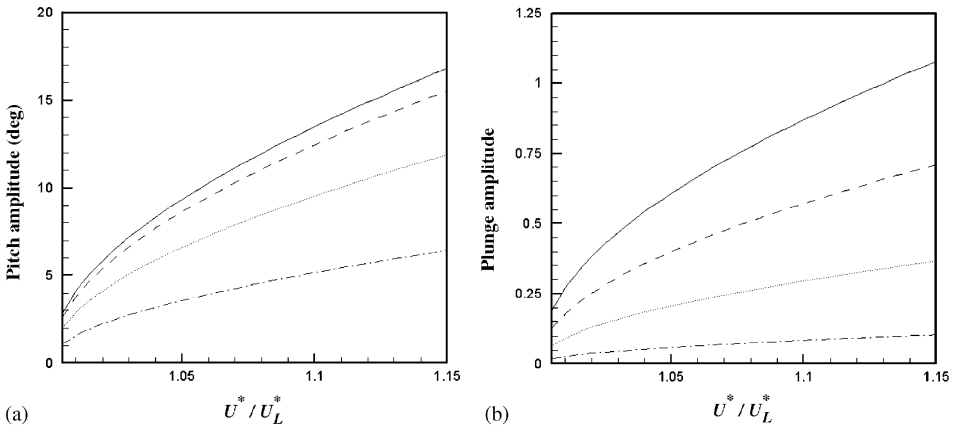

Fig. 8. Dynamical response of different section of the rectangular cantilever wing for Case 2: (a) amplitude of pitch motion; (b) amplitude of plunge motion; – - – -, $\eta = 0.25$; ……, $\eta = 0.5$; – – – , $\eta = 0.75$; —, $\eta = 1.0$.

According to these results, the fifth-order HB method provides very good agreement with the numerical results. Also it should be noted that the accuracy of the HB method is decreased by increasing the U^*/U_L^* ratio.

According to the system of Eqs. (38)–(41) for the first-order HB method (HB1), it is concluded that the LCO frequency is the same for all sections of the rectangular cantilever wing and is independent of the dimensionless parameter η. In Figs. 7 and 8, the LCO plunge and pitch amplitude for different sections of the wing is plotted versus the U^*/U_L^* ratio for Cases 1 and 2 given in Table 4. Since the first plunge and pitch mode shapes of the cantilever beam are used in this research, the maximum and minimum LCO pitch and plunge amplitudes occur at the tip and root of the wing, respectively. So, as shown in Figs. 6 and 7, for the same U^*/U_L^* ratio, the LCO amplitude increases as the dimensionless parameter η increases.

For the wings containing softening cubic nonlinearity, LCO does not occur at speeds beyond the linear flutter boundary. Instead, the flutter phenomenon may occur below the linear flutter boundary as shown in Fig. 10. In Fig. 9 the effect of initial conditions on the nonlinear flutter boundary is shown for Case 3. Because of the nonlinear character of the system, the nonlinear flutter speed is dependent on initial conditions and decreases as the time-dependent part of initial pitch displacement $\alpha_1(0)$ increases.

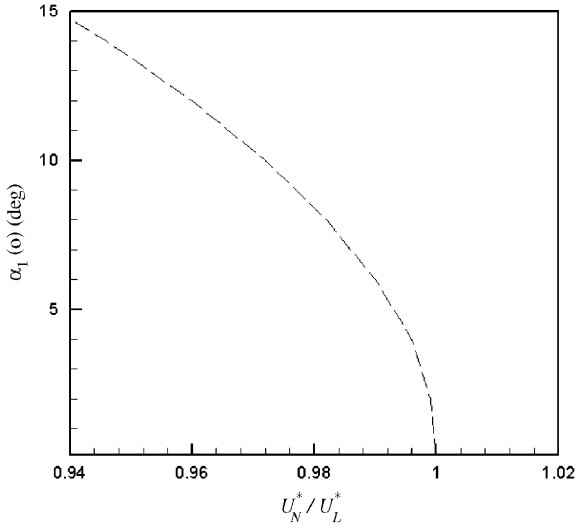

Fig. 9. Diagram of nondimensional nonlinear to linear flutter speed ratio versus initial value of the time-dependent part of pitch motion $\alpha_1(0)$ for Case 3.

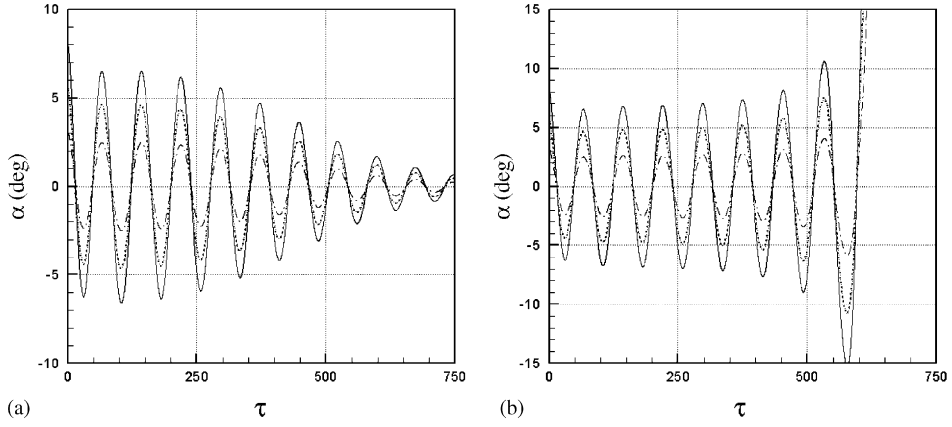

Fig. 10. Pitch displacement versus nondimensional time , τ, at different sections of the wing for Case 3 and $\alpha_1(0) = 8^\circ$: (a) $U^* = 0.981U_L^*$; (b) $U^* = 0.982U_L^*$; – - – -, $\eta = 0.25$; ……, $\eta = 0.5$; —, $\eta = 1.0$.

Similar to the cases with hardening cubic nonlinearity, the nonlinear speed is independent of the dimensionless parameter η. In Fig. 10 for Case 3, diagram of pitch displacement versus nondimensional time τ at speeds below and beyond the nonlinear flutter speed for different sections of the wing are shown. As can be seen, the amplitude of motion increases as η increases.

7. Conclusions

The governing aeroelastic equations of a two-dof rectangular cantilever wing in an incompressible flow were derived in the time domain. In order to verify this formulation, experimental flutter speeds were compared with the results obtained from the derived equations using a time integration method. The results of the presented method are in good agreement with experimental results.

The nonlinear aeroelastic behavior of the two-dof rectangular cantilever wing with hardening and softening cubic nonlinearities was studied in the time domain, and the prediction of LCO amplitude and frequency via the HB method and numerical solution was investigated. The results obtained indicate that:

(i) the amplitude and frequency of LCO are independent of initial conditions;

(ii) the HB method provides accurate predictions for the LCO amplitude and frequency, and the accuracy of the method increases by increasing of its order, as compared to the exact numerical solution;

(iii) the LCO frequency is equal for all sections of the rectangular cantilever wing from root to tip, but the LCO pitch and plunge amplitudes increase for increasing η (dimensionless location of the wing section); the maximum pitch and plunge deflections occur at the wing tip, while their minimum values occur at the root of the wing;

(iv) in the case of softening cubic nonlinearity, the nonlinear flutter which is dependent on initial conditions and independent of the nondimensional term η, can occur below the linear flutter boundary.

Appendix A

The constants $A_1, ..., A_7$ are given below:

$$A_1 = \int_0^1 \left(\frac{\mathrm{d}^2 f_h(\eta)}{\mathrm{d}\eta^2}\right)^2 \mathrm{d}\eta = 22.94429K_1^2, \quad A_2 = \int_0^1 \left(\frac{\mathrm{d}f_\alpha(\eta)}{\mathrm{d}\eta}\right)^2 \mathrm{d}\eta = \frac{\pi^2}{8}K_2^2,$$

$$A_3 = \int_0^1 (f_h(\eta))^2 \,\mathrm{d}\eta = 1.85598K_1^2, \quad A_4 = \int_0^1 (f_\alpha(\eta))^2 \,\mathrm{d}\eta = \frac{K_2^2}{2},$$

$$A_5 = \int_0^1 (f_h(\eta) f_\alpha(\eta)) \,\mathrm{d}\eta = -0.92348K_1K_2.$$

Appendix B

The coefficients of Eqs. (30) and (31) are given as follows:

$$c_0 = A_3 + \frac{A_3}{\mu}, \quad c_1 = A_5 x_\alpha - \frac{1}{\mu} a_h A_5,$$

$$c_2 = 2A_3\zeta_\xi \frac{\bar{\omega}}{U^*} + \frac{2}{\mu}A_3[1 - \psi_1 - \psi_2], \quad c_3 = \frac{1}{\mu}\left[1 + 2(1 - \psi_1 - \psi_2)\left(\frac{1}{2} - a_h\right)\right]A_5,$$

$$c_4 = \frac{2}{\mu}A_3[\psi_1\varepsilon_1 + \psi_2\varepsilon_2], \quad c_5 = \frac{2}{\mu}A_5\left[1 - \psi_1 - \psi_2 + (\psi_1\varepsilon_1 + \psi_2\varepsilon_2)\left(\frac{1}{2} - a_h\right)\right],$$

$$c_6 = \frac{2}{\mu}A_5\left[\psi_1\varepsilon_1 - \psi_1\varepsilon_1^2\left(\frac{1}{2} - a_h\right)\right], \quad c_7 = \frac{2}{\mu}A_5\left[\psi_2\varepsilon_2 - \psi_2\varepsilon_2^2\left(\frac{1}{2} - a_h\right)\right],$$

$$c_8 = -\frac{2}{\mu}A_3[\psi_1\varepsilon_1^2], \quad c_9 = -\frac{2}{\mu}A_3[\psi_2\varepsilon_2^2], \quad d_0 = A_5\left(\frac{x_\alpha}{r_\alpha^2}\right) - \frac{1}{\mu r_\alpha^2}a_h A_5,$$

$$d_1 = A_4 + \frac{1}{\mu r_\alpha^2}\left[a_h^2 + \frac{1}{8}\right]A_4, \quad d_2 = 2A_4\frac{\zeta_\alpha}{U^*} - \frac{(1-2a_h)}{2\mu r_\alpha^2}[(1+2a_h)(1-\psi_1-\psi_2)-1]A_4,$$

$$d_3 = -\frac{2}{\mu r_\alpha^2}\left(\frac{1}{2}+a_h\right)A_4\left[1-\psi_1-\psi_2+(\psi_1\varepsilon_1+\psi_2\varepsilon_2)\left(\frac{1}{2}-a_h\right)\right],$$

$$d_4 = -\frac{2}{\mu r_\alpha^2}\left(\frac{1}{2}+a_h\right)A_5[1-\psi_1-\psi_2], \quad d_5 = -\frac{2}{\mu r_\alpha^2}\left(\frac{1}{2}+a_h\right)A_5[\psi_1\varepsilon_1+\psi_2\varepsilon_2],$$

$$d_6 = -\frac{2}{\mu r_\alpha^2}\left(\frac{1}{2}+a_h\right)A_4\left[\psi_1\varepsilon_1-\psi_1\varepsilon_1^2\left(\frac{1}{2}-a_h\right)\right],$$

$$d_7 = -\frac{2}{\mu r_\alpha^2}\left(\frac{1}{2}+a_h\right)A_4\left[\psi_2\varepsilon_2-\psi_2\varepsilon_2^2\left(\frac{1}{2}-a_h\right)\right],$$

$$d_8 = \frac{2}{\mu r_\alpha^2}\left(\frac{1}{2}+a_h\right)A_5[\psi_1\varepsilon_1^2], \quad d_9 = \frac{2}{\mu r_\alpha^2}\left(\frac{1}{2}+a_h\right)A_5[\psi_2\varepsilon_2^2].$$

Also, the functions $f(\tau)$ and $g(\tau)$ are given below:

$$f(\tau) = \frac{2}{\mu}\left(\left\{A_5\left(\frac{1}{2}-a_h\right)\alpha_1(0) + A_3\xi_1(0)\right\}[\psi_1\varepsilon_1 e^{-\varepsilon_1\tau} + \psi_2\varepsilon_2 e^{-\varepsilon_2\tau}]\right),$$

$$g(\tau) = -\frac{(1+2a_h)}{\mu r_\alpha^2}\left(\left\{A_4\left(\frac{1}{2}-a_h\right)\alpha_1(0) + A_5\xi_1(0)\right\}[\psi_1\varepsilon_1 e^{-\varepsilon_1\tau} + \psi_2\varepsilon_2 e^{-\varepsilon_2\tau}]\right).$$

References

Barmby, J.C., Cunningham, H.J., Garrick, I.E., 1950. Study of effects of sweep on the flutter of cantilever wings. NACA TN 2121.

Dowell, E.H., et al., 2004. A Modern Course in Aeroelasticity. Kluwer Academic Publishers, Dordrecht.

Fung, Y.C., 1969. An Introduction to the Theory of Aeroelasticity. Dover Publications Inc, New York.

Lee, B.H.K., LeBlanc, P., 1986. Flutter analysis of a two-dimensional airfoil with cubic nonlinear restoring force. National Research Council of Canada, Aeronautical Note NAE-AN-36, NRC No. 25438.

Lee, B.H.K., Gong, L., Wong, Y.S., 1997. Analysis and computation of nonlinear dynamic response of a two-degree-of freedom system and its application in aeroelasticity. Journal of Fluids and Structures 11, 225–246.

Lee, B.H.K., Price, S.J., Wong, Y.C., 1999a. Nonlinear aeroelastic analysis of airfoils: bifurcation and chaos. Progress in Aerospace Sciences 35, 205–334.

Lee, B.H.K., Jiang, L.Y., Wong, Y.S., 1999b. Flutter of an airfoil with a cubic nonlinear restoring force. Journal of Fluids and Structures 13, 75–101.

Lee, B.H.K., Liu, L., Chung, K.W., 2005. Airfoil motion in subsonic flow with strong cubic nonlinear restoring forces. Journal of Sound and Vibration 281, 699–717.

Liu, L., Wong, Y.S., Lee, B.H.K., 2000. Application of the center manifold theory in nonlinear aeroelasticity. Journal of Sound and Vibration 234, 641–659.

Marzocca, P., Librescu, L., Silva, W.A., 2002. Aeroelastic response and flutter of swept aircraft wings. AIAA Journal 40, 801–812.

O'Neil, T., Strganac, T.W., 1998. Aeroelastic response of a rigid wing supported by nonlinear springs. Journal of Aircraft 35, 616–622.

Price, S.J., Alighanbari, H., Lee, B.H.K., 1995. The aeroelastic response of a two-dimensional airfoil with bilinear and cubic structural nonlinearities. Journal of Fluids and Structures 9, 175–193.

Shen, S.F., 1959. An approximate analysis of nonlinear flutter problems. Journal of Aerospace Science 26, 25–32.

Woolsten, D.S., Runyan, H.L., Andrews, R.E., 1957. An investigation of effects of certain types of structural nonlinearities on wing and control surface flutter. Journal of Aeronautical Sciences 24, 57–63.